The Astronomical Journal, 130:576–585, 2005 August

THE EFFECT OF SPIRAL STRUCTURE ON THE STELLAR VELOCITY DISTRIBUTION IN THE SOLAR NEIGHBORHOOD

A. C. Quillen and Ivan Minchev
Department of Physics and Astronomy, University of Rochester, Rochester, NY 14627;
aquillen@pas.rochester.edu, iminchev@pas.rochester.edu
Received 2005 February 9; accepted 2005 March 28

ABSTRACT

Clumps in the solar neighborhood's stellar velocity distribution could be caused by spiral density waves. In the solar neighborhood, stellar velocities corresponding to orbits that are nearly closed in the frame rotating with a spiral pattern represent likely regions for stellar concentrations. Via particle integration, we show that orbits can intersect the solar neighborhood when they are excited by Lindblad resonances with a spiral pattern. We find that a two-armed spiral density wave with pattern speed placing the Sun near the 4:1 inner Lindblad resonance can cause two families of nearly closed orbits in the solar neighborhood. One family corresponds to square-shaped orbits aligned so that their peaks lie on top of, and support, the two dominant stellar arms. The second family corresponds to orbits 45° out of phase with the other family. Such a spiral density pattern could account for two major clumps in the solar neighborhood's velocity distribution. The Pleiades/Hyades moving group corresponds to the first family of orbits, and the Coma Berenices moving group corresponds to the second family. This model requires a spiral pattern speed of approximately 0.66 ± 0.03 times the angular rotation rate of the Sun, or 18.1 ± 0.8 km s^{-1} kpc^{-1}.

Key words: Galaxy: disk — Galaxy: kinematics and dynamics — stars: kinematics

1. INTRODUCTION

The velocity distribution of stars in the solar neighborhood contains structure that has been particularly clearly revealed from recent studies of *Hipparcos* observations (Dehnen 1998; Skuljan et al. 1999; Famaey et al. 2005; Chereul et al. 1998, 1999; Nordstrom et al. 2004). Much of this structure was previously identified with moving groups (Eggen 1996). Moving groups are groups of stars that are kinematically associated. Young, early-type stars can be moving together because they carry the kinematic signature of their birth (Eggen 1996). However, a number of the kinematic clumps identified through the kinematic studies also contain later type and older stars (Dehnen 1998; Famaey et al. 2005; Nordstrom et al. 2004). Dubbed superclusters (Famaey et al. 2005; Eggen 1996), these kinematic associations of stars, which are observed all over the sky, can share the same space motions as well-known open clusters. The best documented of the superclusters are the Hyades supercluster associated with the Hyades cluster, the Sirius or Ursa Major supercluster associated with the Ursa Major cluster, and the Pleiades moving group (or Local Association) associated with young clusters such as the Pleiades.

There have been a number of studies exploring the origin of moving groups and superclusters. Eggen (1996) and others have proposed that the structure in the velocity distribution was a result of inhomogeneous star formation and the dissolution of clumps of stars formed simultaneously. Large moving groups could be produced by the dissolution of large stellar agglomerations associated with spiral arms (e.g., Asiain et al. 1999). However, the presence of older stars in the moving groups or superclusters has presented a challenge for this simplest scenario. To account for the older stars, Chereul et al. (1998) suggested that superclusters could be superpositions of moving groups of different age. Because some of the moving groups contain stars spanning a range colors, groups could be long lived and may not necessarily have transient features associated with recently formed clusters that are being disrupted. De Simone et al. (2004) suggested that the clumps in the velocity distribution are due to irregularities in the Galactic potential. In their model, spiral arms near corotation were induced stochastically on a distribution of stellar test particles causing localized structure in the stellar velocity distribution.

The possibility that we consider here is that the clumps in phase space (in the velocity distribution) are associated with or caused by spiral density waves traveling in the solar neighborhood, as discussed by Famaey et al. (2005), Dehnen (1998), and De Simone et al. (2004). This type of explanation would not be unprecedented. The Hercules stream at a tangential velocity of $v \sim 45$ km s^{-1} has been explained in terms of perturbations caused by the Galactic bar (Dehnen 2000; Fux 2001; Raboud et al. 1998). This stream is due to stars in orbits strongly affected by the Galactic bar's 2:1 outer Lindblad resonance. Based on this elegant explanation for the Hercules stream, we are motivated to explore similar explanations for structure in the velocity distribution but at velocities nearer those of circular orbits. Before we consider the effect of spiral density waves on the solar neighborhood's velocity distribution, we first review what is known about the strength, number of arms, and possible pattern speed (angular rotation rate) for spiral density waves likely to be propagating in the solar neighborhood.

The recent study of Vallée (2002) provides a good summary of the many studies that have used observations to map the Milky Way disk. Cepheid, H I, CO, and far-infrared observations suggest that the Milky Way disk contains a four-armed tightly wound structure, whereas Drimmel & Spergel (2001) have shown that the near-infrared observations are consistent with a dominant two-armed structure. The dominant two-armed and weaker four-armed structure was previously proposed by Amaral & Lepine (1997). The nearest spiral arm (excluding the local Orion armlet) is the Sagittarius/Carina arm, 0.9 kpc away from the Sun in the direction toward the Galactic center. The distance between this arm and the Perseus arm in the opposite

direction from us (toward the Galactic anticenter) is about 2.5 kpc.

Based on observational constraints on the Galactic spiral structure, a number of studies have created dynamical models to fit kinematic observations. These models are sensitive to, and so constrain, the spiral pattern speed. Reviewing previous work, Shaviv (2003) finds a clustering of estimates for the pattern speed of local spiral structure near $\Omega_s \sim 20$ km s^{-1} kpc^{-1}, although other studies suggest $\Omega_s \sim 13$ km s^{-1} kpc^{-1}. Lepine et al. (2001) suggest that locally the Milky Way can be modeled by the superposition of a two- and four-armed structure. Their model places the Sun near the corotation resonance ($\Omega_s \sim 28$ km s^{-1} kpc^{-1}) and was fitted to Cepheid kinematics. The recent gas dynamical studies (Martos et al. 2004; Bissantz et al. 2003) match the properties of the gas in nearby arms with a spiral pattern speed of $\sim$20 km s^{-1} kpc^{-1}. Martos et al. (2004) propose that a two-armed stellar structure consistent with the stellar distribution inferred from *COBE* could cause four arms in the gas distribution near the Sun. The gas dynamical model proposed by Bissantz et al. (2003) with a similar spiral pattern speed matches H I and CO kinematics.

In this paper we consider the effect of a spiral density wave on the solar neighborhood velocity distribution. In § 2, we discuss how the velocity components of stars near the Sun are related to their orbits in the Galaxy. In § 3 we describe our technique for determining the velocity components of different populations of stars. In § 4 we explore how different spiral density waves perturb the velocity distribution. A summary and discussion follows.

2. EPICYCLIC MOTION AND THE POSITION ON THE (u, v)-PLANE

We must relate the observed velocities of stars to quantities describing their orbital motion in the Galaxy. The solar neighborhood velocity distribution can be described as a function of the azimuthal velocity component, v, and the radial velocity, $v_r = -u$, where $u > 0$ corresponds to velocities toward the Galactic center. We define v such that the tangential component of the velocity, in the direction of Galactic rotation, is equal to $V_0 + v$, where $V_0 = 220$ km s^{-1} is the local standard of rest at the position of the Sun for a galactocentric radius of $R_0 = 8$ kpc (Reid et al. 1999).

In the absence of perturbations from spiral arms, the motion of stars in the disk of a galaxy can be described in terms of radial or epicyclic oscillations about a circular orbit. It is useful to specify the relation between the observed velocity components u and v and parameters that describe the epicyclic motion. These parameter are the mean radius or guiding radius r_g and the epicyclic amplitude. The energy of an orbit in the plane of an axisymmetric system (neglecting perturbations from spiral structure) is

$$E(u, v) = \frac{(1+v)^2}{2} + \frac{u^2}{2} + \ln r, \tag{1}$$

where the potential energy, $\ln r$, is that appropriate for a flat rotation curve and r is the galactocentric radius. In the above equation we have put velocities in units of V_0 and radii in units of $R_0 = 8.0$ kpc, the distance of the Sun from the Galactic center. The angular rotation rate of a star in a circular orbit at the Sun's radius from the Galactic center, $\Omega_0 = 28$ km s^{-1} kpc^{-1}, is based on observations of the proper motion of Sag A* (Reid et al. 1999) and is consistent with measurements based on Tycho and *Hipparcos* observations (Olling & Dehnen 2003). Hereafter, we place angular rotation rates and pattern speeds in units of Ω_0.

In an epicyclic approximation we can write the energy

$$E = \tfrac{1}{2} + \ln r_g + E_{\rm epi}, \tag{2}$$

where $\frac{1}{2} + \ln r_g$ is the energy of a star in a circular orbit about a guiding radius r_g and $E_{\rm epi}$ is the energy from the epicyclic motion.

$$E_{\rm epi} = \frac{u^2}{2} + \frac{\kappa^2 (r - r_g)^2}{2} = \frac{\kappa^2 a^2}{2}, \tag{3}$$

where a is the epicyclic amplitude and κ is the epicyclic frequency at the guiding or mean radius r_g. We can also write $E_{\rm epi} = j\kappa$, where j is the radial action variable.

We now consider stars specifically in the solar neighborhood, restricting us to a specific location in the Galaxy. The velocity distribution in the solar neighborhood, or the number density of stars as a function of (u, v), is measured near the Sun, where $r \approx 1$ in units of R_0. Using $r = 1$ in equation (1) and setting the energy equal to that written in terms of the epicyclic motion using equations (2) and (3), we solve for r_g. It is convenient to define the distance between the guiding or mean radius and the Sun's galactocentric radius, $s = r_g - 1$. To second order in v, we find that a star near the Sun with velocity components u and v has a guiding radius with

$$s \approx v \tag{4}$$

and epicyclic amplitude

$$a \approx \sqrt{\frac{u^2}{2} + v^2}. \tag{5}$$

The above two relations allow us to relate the velocity components u and v for stars in the solar neighborhood to quantities used to describe the epicyclic motion: the guiding radius and epicyclic amplitude. Particles with positive v have $s > 0$ and so have guiding radii that are larger than R_0 and mean radii outside the Sun's galactocentric radius. Particles with negative v have $s < 0$ and so are expected to spend most of their orbits inside R_0. The distance from the origin $u = v = 0$ determines the epicyclic amplitude.

The angular rotation rate of a star is most sensitive to the value of its guiding radius r_g. The location of Lindblad resonances with a periodic perturbation are therefore primarily set by a star's guiding radius. In the solar neighborhood the guiding radius is primarily dependent on the v velocity component. The location of resonances on the (u, v)-plane is therefore most sensitive to the v value. We focus on the location of resonances because they are one possible cause for the structure in the solar neighborhood velocity distribution. In the vicinity of a resonance there is a bifurcation in the families of periodic orbits and there are *no orbits* that have low epicyclic motion (e.g., Contopoulos 1975). Because resonances can induce large epicyclic (or radial) motions, stars with guiding or mean radii distant from the solar neighborhood could be seen in our vicinity, as is the case for the Hercules stream and the Galactic bar's outer Lindblad resonance.

3. FINDING ORBITS THAT ARE NEAR PERIODIC ORBITS

In this section we describe our numerical procedure for constructing a function that can be compared to the number

density of stars, $f(u, v)\,du\,dv$, in the solar neighborhood. We are restricting this initial study to a spiral perturbation moving at a unique fixed pattern speed or angular rotation rate Ω_s. In this case the Jacobi integral is conserved. By transferring to the frame rotating with the pattern, the Hamiltonian can be brought to a time-independent form (e.g., Binney & Tremaine 1987).

We wish to weight positions in the (u, v)-plane at the position of the Sun according to how likely they are to be occupied by stars. Since stars are born in spiral arms with low velocity dispersion, we assume that they are born in orbits that are nearly periodic or closed in the frame rotating with the arms. After a star is born, it can be scattered by molecular clouds or transient spiral structure as it orbits in the Galaxy. Older stars would occupy orbits that oscillate at a greater extent about the periodic or closed orbits. We have chosen to weight orbits according to how near they are to closed or periodic orbits. Consequently, we construct a numerical way to measure the extent of oscillation about a periodic orbit for stars in the solar neighborhood.

For each position in the (u, v)-plane, we carry out a numerical integration of a particle with initial condition $r = 1, \phi = 0$ corresponding to its location near the Sun. Its initial radial velocity $v_r = -u$, and the tangential velocity is $1 + v$ (in the inertial frame). In the frame rotating with the spiral pattern, we integrate the trajectory of the particle. Each time the particle passes through $\phi = 0$ (the Sun–Galactic center line), we record its position and velocity components. After a specified number of orbits (in most cases 10), we compute the variance of radii (σ_r) and u values (σ_u) at times when the particle passed through $\phi = 0$. The weighting function we used to estimate the likelihood of populating the position in the (u, v)-plane is the sum of these two variances, or $W = \sigma_r + \sigma_u$. We adjusted the number of orbits integrated so that the resulting weighting function was fairly stable; doubling the number of orbits integrated did not result in large changes in W. By keeping the number of integrated orbits low, we could explore a larger region of parameter space.

We use our weighting function to identify locations on the (u, v)-plane likely to be populated with stars. Orbits with initial (u, v)-values that have low values of our weighting function W correspond to orbits where a young star is likely to be born. Older stars could remain in these locations but also would also be scattered out to larger values of W corresponding to locations in the (u, v)-plane with fewer stars.

Our procedure for constructing a weighting function is related to that used to construct surfaces of section. Surfaces of section can be computed by fixing the Jacobi integral and plotting u versus r each time the particle passes through $\phi = 0$ (e.g., Binney & Tremaine 1987). In a surface of section, fixed points correspond to periodic or closed orbits in the galaxy. In such a diagram, our weighting function describes the square of the distance in phase space from a fixed point. We do not use surfaces of section here because they are generated for each value of the Jacobi integral. We wish to study the likelihood of populating orbits as a function of velocity in the solar neighborhood, so we desire a weighting function that is a function of (u, v).

Our method can be compared to the backward integration technique used by Dehnen (2000). Stars at each (u, v) were integrated backward in time, while the Galactic bar was reduced in strength. Velocities on the (u, v)-plane corresponding to orbits with initially low epicyclic motions (before the growth of the bar) were given higher weights (Dehnen 2000). The theory of adiabatic invariants implies that particles with initially low epicyclic motion settle onto periodic or closed orbits following the slow growth of a perturbation. Consequently, we expect that the backward integration method produces weighting contours similar to those of our weighting function. Compared to the backward integration method, our weighting technique has the advantage that it is insensitive to the initial stellar velocity distribution and the manner of perturbation growth (see Fux 2001). These assumptions are a particular problem for spiral density waves, since they could vary in both amplitude (as considered by De Simone et al. 2004) and wavevector or pitch angle (as considered by Fuchs 2001a, 2001b).

Our particle integration is done for particles moving in the plane of the Galaxy. We assume a gravitational potential $V(r, \phi, t) = V_0(r) + V_1(r, \phi, t)$, with $V_0(r) = \ln r$, corresponding to a flat rotation curve. We assume that the gravitational potential perturbation $V_1(r, \phi, t)$ is caused by tightly wound logarithmic spiral density perturbations. Here r and ϕ are the radius and azimuthal angle in the Galactic plane, respectively, and t is time. The potential perturbation can be expanded in terms of Fourier components:

$$V_1(r, \phi, t) = \sum_m A_m \cos[\alpha_m \ln r + m(\phi - \Omega_s t - \gamma_m)]. \quad (6)$$

If only one Fourier component is present, m is the number of arms of that component. The angle γ_m corresponds to an angular offset measured at time $t = 0$. Measured at the Galactic center, γ_m is the angle between the location of the Sun ($r = 1$, $\phi = 0$) and the peak of the spiral pattern at the same radius but at an azimuthal angle differing from that of the Sun. A subsequent figure illustrates this angle. The parameter α_m depends on the pitch angle, p_m, where $\alpha_m = m \cot p_m$. Note that $\alpha_m < 0$ for trailing arms when the rotation is clockwise. Maps of the Milky Way are commonly shown from the viewpoint of an observer located above the Galaxy in the direction of the north Galactic pole (e.g., Drimmel & Spergel 2001; Vallée 2002). On these maps, the rotation is clockwise.

In the WKB or tight-winding approximation, the amplitude of the potential perturbation Fourier component is related to the density perturbations,

$$A_m \sim \frac{-2\pi G \Sigma_0 S_m R_0}{|\alpha_m| V_0^2} \quad (7)$$

(e.g., Binney & Tremaine 1987). In the above equation we have placed A_m in units of V_0^2. Here Σ_m is the amplitude of the mth Fourier component of the spiral mass surface density, and $S_m = \Sigma_m/\Sigma_0$. The mean surface density of disk mass in the solar neighborhood is $\Sigma_0 \sim 50\ M_\odot\ \mathrm{pc}^{-2}$ (Holmberg & Flynn 2000). We estimate for the solar neighborhood

$$A_m \sim 0.03 S_m \left(\frac{\Sigma_0}{50\ M_\odot\ \mathrm{pc}^{-2}}\right) \times \left(\frac{220\ \mathrm{km\ s}^{-1}}{V_0^2}\right)^2 \left(\frac{7}{\alpha_m}\right)\left(\frac{R_0}{8\ \mathrm{kpc}}\right). \quad (8)$$

A two-armed spiral is seen in the near-infrared *COBE* DIRBE data with pitch angle in the range $p \sim 15.^\circ5$–19°, corresponding to $\alpha = m \cot p$ in the range 5.8–7.2 for $m = 2$ (Drimmel & Spergel 2001).

We now estimate ballpark values for the potential perturbation component A_2. Using $S_2 \sim 0.15$, consistent with parameters described by Drimmel & Spergel (2001) for the stellar component (based on K-band observations), equation (8) gives us $A_2 \sim 0.005$. Specifically, Drimmel & Spergel (2001) estimated $(\Sigma_{\max} - \Sigma_{\min})/\Sigma_{\min} = 0.32$, although they suggested that the true value could be higher.

4. STRUCTURE IN THE (u, v)-PLANE

Because the Milky Way has a dominant two-armed spiral pattern, we consider dominant two-armed spiral density waves. In Figure 1 we show the structure of our weighting function $W(u, v)$ for a pure cosine two-armed spiral pattern with the parameters listed in Table 1. Table 1 lists parameters used to describe the spiral perturbation. Each line in the table is labeled with a corresponding figure displaying the output of a simulation.

The strength of the spiral pattern of the simulation shown in Figure 1 is near but somewhat above that estimated by Drimmel & Spergel (2001), with $A_2 = -0.005$. Peaks in density correspond to dips in the gravitational potential. We use negative Fourier amplitudes so that γ_m refers to the location of the peaks (with respect to the Sun) of the spiral density pattern. The density perturbation has the opposite sign to the potential perturbation.

Each panel in Figure 1 corresponds to spiral structure moving at a different pattern speed. We now relate positions in the (u, v)-plane to those expected for Lindblad resonances. The m:1 inner Lindblad resonance (ILR) is located where

$$\Omega_s = \Omega(1 - \sqrt{2}/m) \tag{9}$$

for a flat rotation curve, where $\kappa = \sqrt{2}\Omega$ and Ω and κ are computed as a function of the guiding radius. Here we adopt the notation m:1 ILR referring to m epicyclic oscillations for each orbit around the galaxy in the frame moving with the pattern. Specifically, for the 4:1 ILR, $\Omega_s = 0.65\Omega$; for the 3:1 ILR, $\Omega_s = 0.53\Omega$; and for the 2:1 ILR, $\Omega_s = 0.29\Omega$. The top panel of Figure 1 with $\Omega_s = 0.4$ (in units of Ω_0) has the Sun outside but near the 2:1 ILR. The bottom panel (with $\Omega_s = 0.7$) has the Sun just outside the 4:1 ILR and so nearer to corotation.

In the images shown in Figure 1 the log of our weighting function, $\log_{10} W(u, v)$ is shown in gray scale. Contours are shown with the highest contour with $\log_{10} W = -1$ and a contour interval of 1. The blackest regions correspond to the smallest values of W with $\log_{10} W \sim -4$, which are those most likely to be populated by young stars. These regions could also maintain older stars at low velocity dispersion.

In Figure 1 structure is primarily influenced by the value of v, as expected from our discussion in § 2, since v sets the location of resonances with the spiral pattern. For larger values of v, the angular rotation rate about the Galaxy drops. As v varies, resonances with the spiral perturbation are crossed. Consequently, orbits affected by resonances that have large epicyclic excursions can be seen in the Solar neighborhood.

Dark regions on these diagrams correspond to nearly closed orbits in the frame moving with the spiral pattern. The strongest concentration of closed or periodic orbits in all panels shown in Figure 1 is near the origin where $u = v = 0$ and orbits are nearly circular. When the spiral pattern nears the 2:1 ILR (*top*, with $\Omega_s = 0.4$), the periodic orbits become elongated (highly elliptical), and so their position in the (u, v)-plane is shifted away from the origin. The orbits are elliptical and so have noncircular velocity components. On the lower part of this panel, stars in orbits perpendicular to those supporting the arm can be seen. Stars on these orbits have guiding radii on the other side of the 2:1 ILR.

In these panels, features are also seen at locations separate from the largest concentration at the origin. In the second panel from the bottom, structure is seen near $v \sim 0.05$. In this simulation the Sun is just inside the 4:1 ILR. These orbits correspond to square-shaped orbits, elongated because of this resonance. To illustrate these, we show accompanying orbits for these locations in the (u, v)-plane. In Figure 2 orbits associated with two of the dark regions in this panel are shown. The structure at $v \sim 0.15$ in the panel on Figure 1 corresponds to triangular orbits influenced by the 3:1 ILR. This orbit is also shown in Figure 2.

Nearer to corotation (Fig. 1, *bottom*, at $\Omega_s = 0.7$), orbits above and below the central family are associated with orbits on either side of the 4:1 resonance (supporting and opposite to the pattern). At higher v, higher m Lindblad resonances are encountered closer to the corotation resonance. Here many resonances influence the weighting function and so the model stellar velocity distribution.

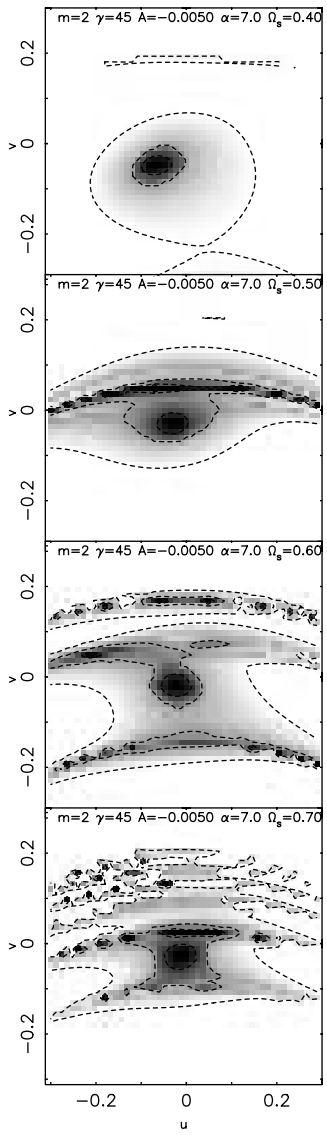

FIG. 1.—The (u, v)-plane for two-armed spiral models at different pattern speeds. The (u, v)-axes are shown in units of V_0, the velocity of a star in a circular orbit at the Sun's galactocentric radius. The gray scale and contours show our weighting function W, which gives a measure of the extent of epicyclic motion about a closed or periodic orbit. From top to bottom, we show the effect of spiral structure with pattern speed $\Omega_s = 0.4, 0.5, 0.6$, and 0.7, respectively (in units of V_0/R_0). The two-armed perturbations have angular offset $\gamma_2 = 45°$, wavevector with $\alpha = 7$, and potential perturbation strength $A_2 = 0.005$ (see Table 1). Dark regions correspond to orbits that are nearly periodic. The top panel is nearest the 2:1 ILR, and so closed or periodic orbits (in the frame of the pattern) are highly elliptical. This causes the periodic orbits to be moderately distant from the origin, where $u = v = 0$ and where circular orbits are located in the absence of spiral perturbations. The bottom panel is near the outside of the 4:1 Lindblad resonance. The structure at low v in the bottom panel is caused by the 4:1 Lindblad resonance. At larger v, structure from higher m Lindblad resonances is encountered closer to corotation.

TABLE 1
PARAMETERS DESCRIBING SPIRAL PATTERNS

Figures	A_2	γ_2 (deg)	α_2	Ω_s
1.....	−0.005	45	−7	0.4, 0.5, 0.6, 0.7
2.....	−0.005	45	−7	0.6
3.....	−0.008	15, 30, 45, 60, 75	−6	0.60, 0.625, 0.65, 0.675
4, 5, 6.....	−0.008	15	−6	0.675

NOTES.—These are the parameters of the spiral pattern corresponding to simulations shown in the figures. The angular offset γ_2 is the angle (measured at the Galactic center) between the location of the Sun and the nearest density maximum of the spiral potential perturbation at a radius of R_0 (see Fig. 5). The perturbation strength A_2 is given in units of V_0^2, the velocity of a star in a circular orbit at R_0. The pattern speed, Ω_s, is given in units of $\Omega_0 = V_0/R_0$. The parameter α_2 sets the pitch angle of the spiral arms. For $\alpha_2 < 0$, the arms are trailing when the rotation is clockwise.

4.1. *Near the 4:1 Inner Lindblad Resonance*

In the previous section we discussed two-armed patterns over a large range of pattern speeds but at only one angular offset, $\gamma_2 = 45^\circ$. We noted in Figure 1 that at higher pattern speeds more structure appears in the weighting function on the (u, v)-plane, as higher m Lindblad resonances are encountered closer to corotation. In this section we consider in more detail the possible role of the 4:1 ILR. Because square-shaped orbits are excited near this resonance, we expect that the velocity distribution could depend strongly on the orientation of the spiral pattern. Therefore, we must consider the sensitivity as a function of the angular offset γ_2.

In Figure 3 weighting on the (u, v)-plane is shown for a somewhat stronger two-armed spiral pattern. Parameters for the spiral pattern are listed in Table 1. From top to bottom in these panels, the angular offset between the spiral maximum and the Sun $\gamma_2 = 15^\circ$, 30°, 45°, 60°, and 75°. From left to right in this figure, the spiral pattern speed $\Omega_s = 0.60, 0.625, 0.65$, and 0.675. In Figure 3 we note that a wealth of structure exists in these plots, particularly for the pattern speeds near and above the 4:1 ILR at $\Omega_s \approx 0.65$.

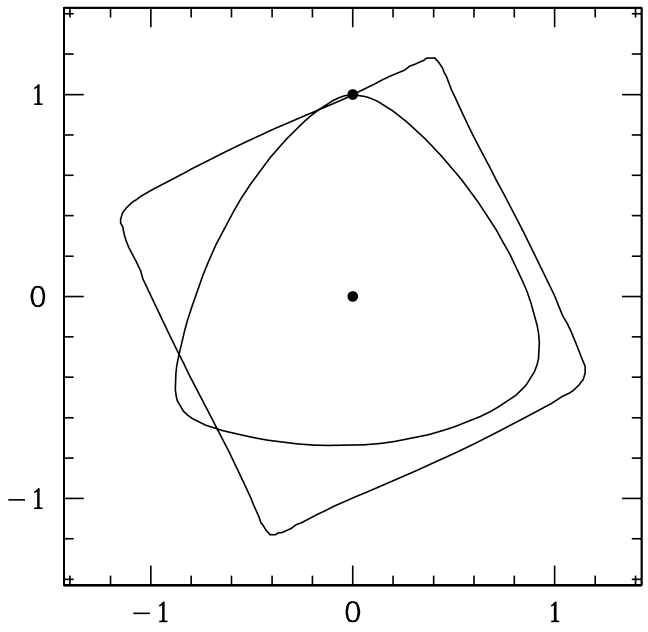

FIG. 2.—Closed orbits in the frame moving with the spiral structure for the two-armed $\Omega_s = 0.60$ model (see Table 1 for parameters). The weighting function for this model is shown in the second panel from the bottom in Fig. 1. Orbits are shown for two dark regions in this panel. The triangular closed orbit corresponds to a position on the (u, v)-plane with $u = 0.00$, $v = -0.15$. The square orbit corresponds to $u = -0.20$, $v = 0.05$.

If the spiral pattern places the Sun near its 4:1 ILR, we see that two dominant clumps in the weighting function appear near the origin in the (u, v)-plane for low values of γ_2 (Fig. 3, *top panels of right two columns*). In Figure 4 we show the shape of closed orbits (in the frame rotating with the pattern) for these two clumps for $\gamma_2 = 15^\circ$ and $\Omega_s = 0.675$ (also see Table 1). Orbits are plotted for $(u, v) = (-0.065, -0.043)$, the inner diamond orbit, and $(u, v) = (0.025, 0.015)$, the outer rectangular orbit. The inner orbits would have density peaks at the location of two of the density peaks aligned with the density perturbation. Consequently, we say they support the spiral pattern. The outer orbits have guiding radii on the other side of the 4:1 ILR and so are out of phase with the inner orbits.

As pointed out by previous works, two-armed density perturbations can excite square-shaped orbits (Contopoulos & Grosbol 1986) and a four-armed gaseous response (Martos et al. 2004) near the 4:1 ILR. At guiding radii exterior to the 4:1 ILR, a pure $m = 4$ potential perturbation (with potential components $A_4 \neq 0$ and $A_2 = 0$) excites orbits that support the spiral pattern. Interior to the 4:1 ILR, the closed orbits would be out of phase with the density perturbation and so would fail to support the spiral pattern. The orientation or phase of the orbits changes at the resonance. When the orbits support the spiral pattern, they lie on top of the perturbation in such a way that a self-consistent model can be created. In other words, the density perturbation causes orbit perturbations that in turn are consistent with the density perturbation. When there is only a strong two-armed potential perturbation, as is the case currently discussed here, the orbits can still be strongly influenced by the 4:1 ILR. In this case, the 4:1 ILR is of the second order in the epicyclic amplitude ($\propto j$ rather than $j^{1/2}$; Contopoulos & Grosbol 1986). Again, the closed orbits can be square-shaped near the 4:1 ILR but are oriented so that they support the spiral pattern *interior* to the 4:1 ILR and fail to support the pattern *exterior* to the 4:1 ILR. The tendency for orbits to fail to support spiral structure outside the 4:1 ILR prompted Contopoulos (1985) to propose that two-armed spiral patterns end near their 4:1 ILRs (also see Contopoulos & Grosbol 1986; Patsis & Kaufmann 1999).

We now compare the structure seen in Figure 3 with the velocity components of moving groups. In our units, dominant moving groups in the solar neighborhood velocity distribution have velocity components $(u, v) = (-0.05, -0.10)$ for the Pleiades moving group, $(-0.18, -0.09)$ for the Hyades moving group, $(-0.04, -0.02)$ for the Coma Berenices moving group, and (0.04, 0.01) for the Sirius/Ursa Major moving group. These velocity components are based on the stellar distribution measured with *Hipparcos* observations and are given with respect to the Sun by Dehnen (1998). The study by Famaey et al. (2005)

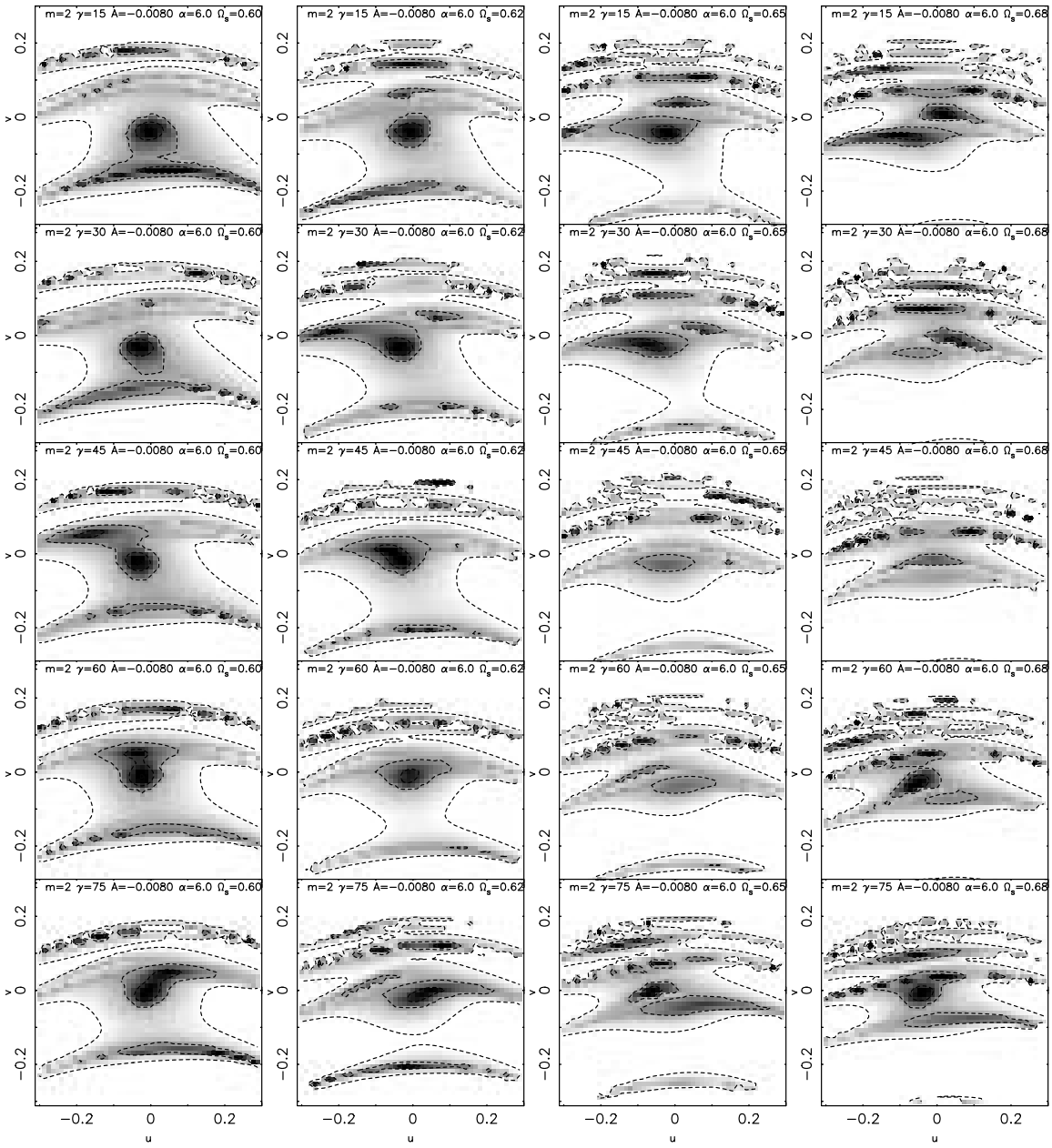

FIG. 3.—The (u, v)-plane for stronger two-armed spiral models at pattern speeds placing the Sun near the 4:1 ILR. Panels are similar to those shown in Fig. 1. From left to right, the pattern speed is $\Omega_s = 0.60, 0.625, 0.65$, and 0.675, respectively. In each column, from top to bottom, the angle of the spiral pattern with respect to the Sun is $\gamma_s = 15^\circ$, 30°, 45°, 60°, and 75°, respectively. Parameters for these simulations are also listed in Table 1.

grouped the Pleiades and Hyades moving groups together and identified the Coma Berenices and Sirius/Ursa Major groups as separate structures. Note that we have divided the velocities by V_0.

Based on the right two columns in Figure 3, which are at pattern speeds $\Omega_s = 0.65$ and 0.675 near the 4:1 IRL, it is attractive to associate the Pleiades/Hyades moving group with the nearly closed orbits at $v \sim -0.05$ and the Coma Berenices moving group with the nearly closed orbits near the origin ($u \sim v \sim 0$). For $\gamma_2 \sim 15^\circ$, the (u, v)-weighting function shows an extension to low u for the lower clump, suggesting that low-oscillation orbits exist over an elliptical region in the (u, v)-plane that could encompass both the Hyades and Pleiades moving groups. If this choice of spiral perturbation accounts for the Hyades/Pleiades and Coma Berenices moving groups, then the Hyades/Pleiades moving group stars are in orbits oscillating about the interior diamond-shaped closed orbit passing through the solar neighborhood (see Fig. 4) and the Coma Berenices group stars are near the outer rectangular closed orbit. We note that both families of closed orbits are elongated or not perfectly square. This would be expected because the potential perturbation is elliptical or two-armed. The square shape of these closed orbits is a result of the proximity of the 4:1 ILR.

We have found that the 4:1 ILR provides a promising explanation for some of the structure in the solar neighborhood velocity distribution. If a spiral density wave can produce this structure, then it should be consistent with the location of spiral arms near the Sun. We now consider the location of the spiral arms for a model that could account for the Hyades/Pleiades and Coma Berenices moving groups. Of the panels shown in Figure 3, we choose that with $\Omega_s = 0.675$ and $\gamma_2 = 15^\circ$. The position of the two spiral arm density peaks consistent with this model are shown as solid lines in Figure 5. If there were an

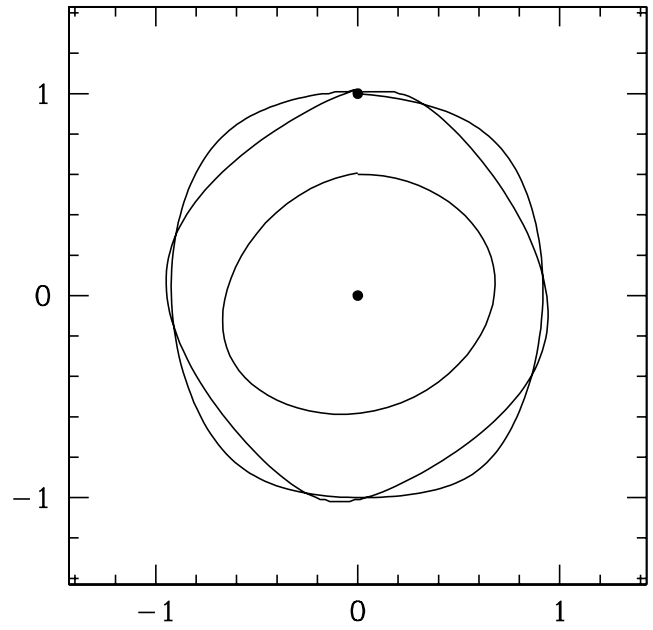

FIG. 4.—Closed orbits in the frame moving with the spiral structure for the two-armed $\Omega_s = 0.675$ model (see Table 1 for parameters). The weighting function for this model is shown in the top panel in the third column from the left in Fig. 3. Orbits are shown for two dark regions in this panel at the location of the Sun. The inner square closed orbit corresponds to a position on the (u, v)-plane with $u = -0.065$, $v = -0.043$. This orbit supports (lies on top of) the dominant two-armed perturbation. In other words, two of the orbit peaks are on top of two of the arms. The outer, rounder square orbit corresponds to $u = 0.025$, $v = 0.015$ and is out of phase with the two-armed density perturbation. We also show an inner orbit supporting the two arms inside the galactocentric radius of the Sun.

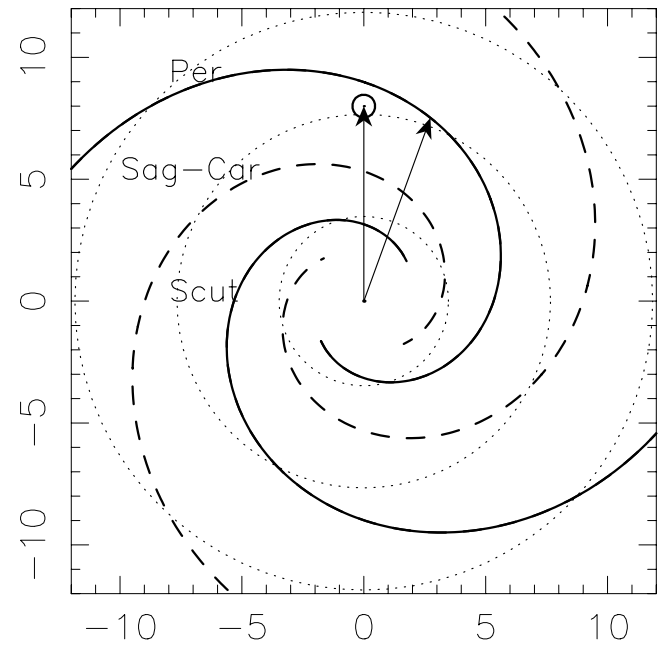

FIG. 5.—Location of arms with respect to the Sun consistent with the distributions shown in Fig. 3 (*top panels*) with $\gamma_2 = 15°$. The two stellar arms are shown as solid lines. If two additional arms were present between the two strong stellar ones, they would be located approximately at the dashed lines. The position of the Sun is shown as a small circle. The location of the 2:1 ILR, 4:1 ILR, and corotation resonance are shown as large dotted circles. The angle between the Sun and the nearest strong arm, γ_2, is that between the two vectors. We have labeled the arms according to their common names. In this figure Galactic rotation is clockwise. See Table 1 for descriptions of the parameters.

additional two arms located in between the dominant two stellar ones, they would be located where the dotted lines are shown on Figure 5. Axes on this figure are given in kiloparsecs so that the spiral arms in the model can be compared with the location of observed arms (based on names referred to by Vallée 2002).

From Figure 5 we see that our spiral model successfully places the Sun between the Perseus and Sagittarius/Carina arms. We have adjusted the pitch angle of the spiral arms (set α) so that the separation between the Perseus arm and the Sagittarius/Carina arm is consistent with that suggested by Vallée (2002). However, our model requires that the Sun is closer to the Perseus arm than the likely location of the Sagittarius/Carina arm, in contradiction to the model by Vallée (2002). We note that the Sagittarius/Carina arm is not as strong in stars as it is in gas (Drimmel & Spergel 2001), and the dust map of Drimmel & Spergel (2001) shows a kink or bend in the Sagittarius/Carina near the Sun. This bend may be associated with the change in the orbit structure at the 4:1 ILR. The model of Vallée (2002) assume a purely logarithmic shape for the spiral arms, whereas the orbit structure near the 4:1 probably causes deviations in the location of the arms. Fourier decomposition of nearby galaxy images has shown that even when the galaxy is grand design, Fourier components with $m > 2$ may still be significant (e.g., Elmegreen et al. 1992; Seigar & James 1998; Grosbol et al. 2004), and the simple model explored here only considers a dominant $m = 2$ Fourier component. A more detailed model for the arms (based on the observations) and a self-consistent model for the spiral arms, the gas response, and population of orbits would be required to determine whether the arm locations were consistent with the proposed dynamical model.

We now discuss the sensitivity of our proposed spiral wave model to the parameters used to define it. We have carried out comparison simulations with different spiral arm pitch angles. We find that the weighting function contours (and inferred structure in the velocity distribution) are not strongly sensitive to the value of α_2. For α_2 between 5 and 7, consistent with the range of pitch angles discussed by Drimmel & Spergel (2001) and Vallée (2002), little difference is seen the structure of the weighting function. However, from Figure 3 it is clear that the model velocity distribution (and orbital structure) is very sensitive to the orientation angle of the spiral arms (γ_2) with respect to the Sun. Changes in γ_2 of as small as 10° can cause significant changes in the locations of closed orbits in the solar neighborhood.

We have also varied the strength of the two-armed perturbation, A_2. For $|A_2| < 0.005$, the orbits are more nearly circular and would not be able to be consistent with two dominant spiral arms (the orbits are not sufficiently elliptical away from the 2:1 ILR). For $|A_2| < 0.005$ the width of the 4:1 ILR is smaller (the resonance is second order in the epicyclic amplitude) and the two families of orbits near the 4:1 ILR are closer together, too close to account for the Hyades/Pleiades and Coma Berenices moving group separations. For $|A_2| > 0.01$, the separation between the two orbit families was larger than that of the two moving groups. We had best results finding a model (u, v)-distribution similar to that observed in the solar neighborhood for $A_2 \sim 0.008 \pm 0.002$. We note that this is about twice as high as that estimated from the K-band model by Drimmel & Spergel (2001). Specifically, Drimmel & Spergel (2001) estimated $(\Sigma_{\max} - \Sigma_{\min})/\Sigma_{\min} = 0.32$, which is smaller than the contrast seen in other similar nearby galaxies (Seigar & James 1998; Grosbol et al. 2004). Consequently, Drimmel & Spergel (2001) commented that they suspected the true value for the density contrast (arm vs. interarm) could be higher than this number.

In Figure 6 we directly compare our model (see Table 1 for parameters) (u, v)-plane panel, showing our weighting function,

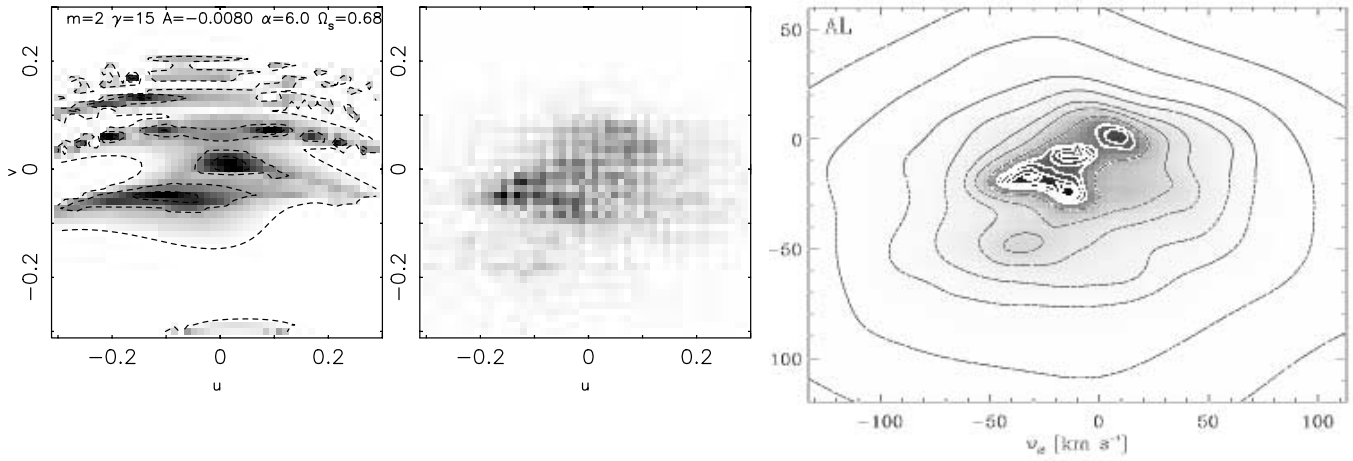

FIG. 6.—Comparison between our model for the (u, v)-plane (*left*) and the observed stellar velocity distribution. The left panel (similar to Fig. 1) has parameters listed in Table 1. The middle panel is a two-dimensional histogram of the (u, v)-velocities of the F and G dwarf stars listed by Nordstrom et al. (2004) in units of V_0. The (u, v)-velocity components listed in Table 1 by Nordstrom et al. (2004) are heliocentric. To compare these velocities to those shown in the left panel, we have assumed a $V_{\rm LSR}$ velocity of $U_0 \approx V_0 \approx 8$ km s^{-1}. The right panel is from Dehnen (1998), Fig. 3, for all stars in his *Hipparcos* subsample. In the right panel, the clump nearest the origin is the Coma Berenices moving group. The clump below the Coma Berenices group is the Pleiades moving group. The clump at positive velocities is the Sirius/Ursa Major moving group, and the clump at $v = -40$ km s^{-1} is the Hyades moving group. We note that our model predicts that the Hyades and Pleiades moving groups are kinematically related. This is consistent with the study by Famaey et al. (2005), which found no strong separation between them. Our model is consistent with the velocity separation between the Coma Berenices and Hyades/Pleiades moving groups and predicts a slight tilt (larger v for more negative u) to the Hyades/Pleiades moving groups contours that is seen in the observed velocity distribution. In our model, the Hyades/Pleiades stars are on diamond-shaped orbits, supporting the spiral pattern, and those in the Coma Berenices group are on orbits that are out of phase by 45°. The Hyades/Pleiades stars have mean radii that are within the Sun's galactocentric radius. Those at larger v have mean radii outside R_0.

to the observed stellar velocity distribution in the solar neighborhood. The middle panel on this figure is the stellar velocity distribution of the F and G dwarf stars listed by Nordstrom et al. (2004). The right-hand panel of this figure is from Figure 3 of Dehnen (1998), which shows all stars in his *Hipparcos* sample. This panel from Figure 3 by Dehnen (1998) resembles Figure 20 by Nordstrom et al. (2004) and Figure 7 from Famaey et al. (2005). In our panel the origin corresponds to a circular orbit in the absence of perturbations by spiral arms; however, the stellar velocity distribution is plotted with respect to the solar velocity. If our proposed dynamical model is correct, it suggests that the Sun is moving with $(u, v) > 0$.

In the figure by Dehnen (1998), the clump nearest the origin is the Coma Berenices moving group. The clump below the Coma Berenices group is the Pleiades moving group. The clump at positive velocities is the Sirius/Ursa Major moving group, and the clump at $v = -40$ km s^{-1} is the Hyades moving group. We note that our model predicts that the Hyades and Pleiades moving groups are kinematically related. This is consistent with the studies by Famaey et al. (2005) and Nordstrom et al. (2004), which found no strong separation between them. Our model is consistent with the velocity separation between the Coma Berenices and Hyades/Pleiades moving groups and predicts a slight tilt (larger v for more negative u) to the Hyades/Pleiades moving group contours that is seen in the observed velocity distribution.

Based on the comparison between our model and the observed velocity distribution, it is tempting to associate the Sirius/Ursa Major moving group with closed orbits at higher v that would correspond to higher m ILRs. However, since these would be affected by higher m resonances, the structure of the orbits is likely to be very strongly dependent on the location of the Sun with respect to the spiral structure and on the assumed structure of the spiral arms. Consequently, we do not feel we can attach any significance to structure in our model at the location of the Sirius/Ursa Major moving group. If higher order resonances affect stars with guiding radii just outside the Sun, then it is possible that the outer Milky Way disk is flocculent (Quillen 2002). It is also possible that an additional spiral density wave could affect the outer part of the galaxy, adding an additional complication that we have not explored here.

The 4:1 Lindblad resonance provides an explanation for some of the structure present in the stellar velocity distribution in the solar neighborhood. However, this explanation succeeds only over a very narrow range of pattern speeds. For the small range of reasonable perturbation strengths, based on the structure seen in Figure 3, we estimate that the spiral pattern speed must be within $\Omega_s = 0.66 \pm 0.03$. This corresponds to a pattern speed of $\Omega_s = 18.1 \pm 0.8$ km s^{-1} kpc^{-1} (after restoring the physical units). This pattern speed is consistent with many previous estimates (Shaviv 2003) and the kinematic models by Martos et al. (2004) and Bissantz et al. (2003). Our model for the velocity distribution is quite similar to that of Martos et al. (2004), who showed that a dominant two-armed stellar perturbation could cause four arms in the gas distribution.

5. SUMMARY AND DISCUSSION

In this paper we have considered the effect of spiral density waves on structure in the stellar velocity distribution in the solar neighborhood. We find that Lindblad resonances with spiral density waves can cause structure in the velocity distribution. Lindblad resonances can excite large epicyclic perturbations, allowing stars from distant locations to reach the solar neighborhood. In the solar neighborhood, we find that the location of a resonance is primarily set by the tangential velocity component, v. Because spiral perturbations are not strong, their widths are narrow and they only excite large epicyclic oscillations over a narrow range of guiding or mean radii. However, because these epicyclic oscillations can cause stars to cross into the solar neighborhood, they can still cause structure in the solar neighborhood velocity distribution.

Because Lindblad resonances can cause significant changes in the structure of orbits, they provide a promising explanation

for structure seen in the solar neighborhood velocity distribution or moving groups and superclusters. To explore this possibility, we have searched for orbits that are near closed or periodic orbits in the frame moving with the spiral pattern. We have constructed a weighting function that estimates the distance in phase space of an orbit from a closed or periodic orbit. When a moderately strong two-armed perturbation is present with pattern speed at 0.66 ± 0.03 times the angular rotation rate of the Sun, placing the Sun near the 4:1 Lindblad resonance, two regions near the origin in the (u, v)-plane exhibit nearly closed orbits. These islands are likely to be populated by stars spanning a range of ages, as are moving groups.

For a two-armed model with pattern speed placing the Sun near the 4:1 Lindblad resonance and an angular offset of $\gamma_2 = 15^\circ$, the structure of our weighting function resembles the observed velocity distribution. Nearly closed orbits are located near existing moving groups. The region at negative v in the (u, v)-plane is elongated toward negative u and so could encompass both the Hyades and Pleiades moving groups. The region at positive v can be associated with the Coma Berenices moving group. This model provides a possible explanation for some of the structure observed in the solar neighborhood's velocity distribution. The model succeeds only over a very narrow range of pattern speeds, with $\Omega_s = 18.1 \pm 0.8$ km s^{-1} kpc^{-1} providing a tight constraint on the angular rotation rate of the spiral pattern. Our model is most similar to and consistent with the model proposed by Martos et al. (2004), in which two dominant stellar arms excite a four-armed gaseous response.

We have shown here that resonances with spiral patterns provide a promising way to explain clumps in the solar neighborhood velocity distribution. In this paper we have only considered the response of stars to spiral density perturbations but did not consider the response of the gas. In our model, we have not constructed a stellar orbit distribution consistent with the assumed density perturbation. Future work should strive to create models that are more self-consistent. Here we have not explored the sensitivity of the stellar distribution with stellar birth site or age. However, Dehnen (1998) and Famaey et al. (2005) found that structure in the velocity distribution depends on the type of star or stellar population. Here we used a crude weighting function to find nearly periodic orbits in the (u, v)-plane; however, we have not produced model stellar density distributions. Future work could consider the birth of stars in a disk supporting a spiral pattern and explore ways to predict the location and number of stars as a function of birth site and age. Future work could also consider the sensitivity of the present-day velocity distribution to the way that spiral structure evolves. For example, it may be possible to differentiate between pure amplitude growth (as considered by De Simone et al. 2004) from shearing density wave models for which both amplitude and wavevector vary simultaneously (e.g., as considered by Fuchs 2001a, 2001b).

There are some interesting consequences of our model. The 4:1 resonance is likely to cause deviations from a pure logarithmic spiral pattern near the Sun. Better models for the Galaxy could include arms that deviate from logarithmic spirals. Because the Sun may be located near a Lindblad resonance causing large epicyclic amplitudes in the stars, measurements of the velocity of the local standard of rest ($V_{\rm LSR}$) and Oort's constants are likely to be biased. By understanding and correcting for these biases, measurements of these astronomical quantities may be improved. In this paper we have not proposed a dynamical explanation for the Sirius/Ursa Major moving group. This group could be related to a higher m Lindblad resonance, or perhaps there is another spiral density wave moving at a slower pattern speed at larger galactocentric radius. Here we have suggested that the Hyades/Pleiades moving groups are on orbits with mean radii within the Sun's galactocentric radius and the Coma Berenices and Sirius/Ursa Major moving groups are on orbits with mean or guiding radii outside R_0. It would be interesting to see if these stellar populations have different age and metallicity distributions. Here we have not discussed the orbits of stars at velocities between the moving groups. Because of the 4:1 ILR, these stars should have large epicyclic amplitudes and so could be part of a different stellar population than the moving groups.

Here we have not considered the role of more than one spiral density wave or the role of the Galactic bar. Stellar orbits that are not affected by a Lindblad resonance from an additional perturbation, such as from another spiral density wave or the Galactic bar, would be only weakly affected by the additional perturbation. Away from a resonance, the orbital kinematics can be treated with low-order perturbation theory (for example, as done by Binney & Tremaine 1987). Only stars (at $v \sim 50$ km s^{-1}) associated with the Hercules stream that are influenced by the bar's 2:1 Lindblad resonance should be strongly affected by the Galactic bar. Stars at lower values of $(|u|, |v|)$ should be distant and so unaffected by Lindblad resonances with the Galactic bar. We expect that the closed orbits considered in this paper weakly oscillate or are weakly perturbed at the frequency of the Galactic bar. These oscillations should cause small variations in the location of the periodic orbits on the (u, v)-plane as seen from the solar neighborhood. However, as long as we consider orbits that are not associated with resonances with the Galactic bar, then strong features associated with the bar would not be seen in the velocity distribution. The same situation is likely if there is an additional spiral density wave (at a different pattern speed) present in the solar neighborhood (as suggested most recently by Naoz & Shaviv 2005). We only expect strong structures in the velocity distribution that are associated with resonances from one of the spiral density waves present in the solar neighborhood. However, the presence of more than one perturbation can influence the stellar dynamics. For example, if the solar neighborhood is affected by more than one spiral density wave, then stars at velocities between moving groups might be on chaotic orbits (Quillen 2003), a factor that could cause a relatively large increase in their velocity dispersion with time.

This work could not have been carried out without helpful discussions with Larry Helfer and Don Garnett. We thank the referee, B. Fuchs, for helpful comments that have improved the manuscript. A. C. Q. gratefully thanks the Technion for hospitality and support during the fall of 2001 when this project was initiated.

REFERENCES

Amaral, L. H., & Lepine, J. R. D. 1997, MNRAS, 286, 885
Asiain, R., Figueras, F., & Torra, J. 1999, A&A, 350, 434
Binney, J., & Tremaine, S. 1987, Galactic Dynamics (Princeton: Princeton Univ. Press)
Bissantz, N., Englmaier, P., & Gerhard, O. 2003, MNRAS, 340, 949
Chereul, E., Creze, M., & Bienayme, O. 1998, A&A, 340, 384
———. 1999, A&AS, 135, 5
Contopoulos, G. 1975, ApJ, 201, 566
———. 1985, Comments Astrophys., 11, 1
Contopoulos, G., & Grosbol, P. 1986, A&A, 155, 11

Dehnen, W. 1998, AJ, 115, 2384
———. 2000, AJ, 119, 800
De Simone, R. S., Wu, X., & Tremaine, S. 2004, MNRAS, 350, 627
Drimmel, R., & Spergel, D. N. 2001, ApJ, 556, 181
Eggen, O. J. 1996, AJ, 112, 1595
Elmegreen, B. G., Elmegreen, D. M., & Montenegro, L. 1992, ApJS, 79, 37
Famaey, B., Jorrissen, A., Luri, X., Mayor, M., Udry, S., Dejonghe, H., & Turon, C. 2005, A&A, 430, 165
Fuchs, B. 2001a, A&A, 368, 107
———. 2001b, MNRAS, 325, 1637
Fux, R. 2001, A&A, 373, 511
Grosbol, P., Patsis, P. A., & Pompei, E. 2004, A&A, 423, 849
Holmberg, J., & Flynn, C. 2000, MNRAS, 313, 209
Lepine, J. R. D., Mishurov, Y. N., & Dedikov, S. Y. 2001, ApJ, 546, 234
Martos, M., Hernadez, X., Yanez, M., Moreno, E., & Pichardo, B. 2004, MNRAS, 350, L47
Naoz, S., & Shaviv, N. J. 2005, ApJ, submitted (astro-ph/0503127)
Nordstrom, B., et al. 2004, A&A, 418, 989
Olling, R. P., & Dehnen, W. 2003, ApJ, 599, 275
Patsis, P. A., & Kaufmann, D. E. 1999, A&A, 352, 469
Quillen, A. C. 2002, AJ, 124, 924
———. 2003, AJ, 125, 785
Raboud, D., Grenon, M., Martinet, L., Fux, R., & Udry, S. 1998, A&A, 335, L61
Reid, M. J., Readhead, A. C. S., Vermeulen, R. C., & Treuhaft, R. N. 1999, ApJ, 524, 816
Seigar, M. S., & James, P. A. 1998, MNRAS, 299, 685
Shaviv, N. J. 2003, NewA, 8, 39
Skuljan, J., Hearnshaw, J. B., & Cottrell, P. L. 1999, MNRAS, 308, 731
Vallée, J. P. 2002, ApJ, 566, 261